Research Square

Preprints are preliminary reports that have not undergone peer review.
They should not be considered conclusive, used to inform clinical practice,
or referenced by the media as validated information.

Atmospheric cold plasma modifies technological and macromolecular properties of local Tarom rice: Comparison with Traditional Processing Methods

Javaneh Karimi
Shahid Sadoughi University of Medical Sciences
Mohammad Zabihinpour
Payame Noor University
Reyhaneh Sefidkar
Shahid Sadoughi University of Medical Sciences
Neda Mollakhalili-Meybodi
neda_mabodi@yahoo.com

Shahid Sadoughi University of Medical Sciences and Health Services
Reza Esmaeilzadeh Kenari
Sari Agriculture and Natural Resources University

Article

Keywords: atmospheric cold plasma, rice, starch, glutelin, cooking quality, nonthermal processing

Posted Date: November 19th, 2026

DOI: https://doi.org/10.21203/rs.3.rs-11597246/v1

License: This work is licensed under a Creative Commons Attribution 4.0 International License.
Read Full License

Additional Declarations: Competing interest reported. This research received financial support from Shahid Sadoughi University of Medical Sciences, Yazd, Iran, as part of the corresponding thesis project. No grant number was assigned to this funding.

Abstract

Atmospheric cold plasma (ACP) offers a nonthermal alternative to parboiling for modifying rice quality. *Local Tarom* rice was treated with ACP for 30, 60, 90, or 120 s and compared with parboiled and untreated controls. Moisture content, cooking properties, Fourier-transform infrared spectra, X-ray diffraction, atomic force microscopy, color, differential scanning calorimetry, and glutelin circular dichroism were evaluated. ACP produced treatment-time-dependent effects. Treatment for 90 s yielded the shortest minimum cooking time (1352.753 ± 30.692 s) without significantly altering water absorption or solid loss. This treatment also produced the greatest surface height and roughness, while the A-type starch crystalline pattern was retained and glutelin secondary structure remained stable. Compared with parboiling, ACP caused less pronounced color change. These findings indicate that ACP treatment for 90 s can improve the cooking performance of Tarom rice primarily through controlled surface modification while preserving major starch and protein structural features.

Introduction

Rice (*Oryza sativa L.*) is one of the most important food grains worldwide and is the staple food for nearly half of the global population [1]. It is an important source of complex carbohydrates (64.21–71.09 g/100 g), protein (6.79–10.74 g/100 g), fat (0.31–1.69 g/100 g), dietary fiber (2.59–3.92 g/100 g), minerals, and vitamins [2–4]. Approximately 80% of the world's rice is consumed in Asia [5]. In many regions, rice is commonly consumed as white rice, in which the bran and germ are removed during milling. This process improves appearance and palatability but causes losses of several nutritional and bioactive components [6,7]. The technological quality of rice is mainly determined by the structural organization of starch and protein, their interactions within the endosperm matrix, and the extent to which these macromolecules remain intact during milling and subsequent processing. Starch, as the major component of milled rice, strongly influences gelatinization behavior, water uptake, texture, and cooking quality, while protein can restrict starch swelling and affect grain hardness and cooking performance. Therefore, maintaining the integrity of starch–protein organization is essential for preserving desirable technological properties of rice during processing [1]. In contrast, parboiling can improve some nutritional and technological attributes by promoting the migration of soluble compounds from the bran layer into the endosperm [4]. Parboiling has been proposed as an effective hydrothermal process to improve rice technological quality because it promotes starch gelatinization, reduces kernel fissuring, and helps preserve grain integrity during milling. However, conventional parboiling is energy-intensive, generates wastewater, and may cause undesirable changes such as yellowing, darkening, and texture modification. Accordingly, recent studies have increasingly focused on atmospheric cold plasma (ACP), a nonthermal and environmentally friendly approach that can reduce microbial contamination, modify surface properties, improve hydration behavior, and stimulate seed-related responses without severe nutrient degradation [8–10].

ACP is a partially ionized gas containing ions, free electrons, neutral atoms, excited molecules, ultraviolet photons, and reactive oxygen and nitrogen species [11,12]. These reactive species can interact with biological macromolecules and grain surfaces, mainly through plasma etching, limited oxidation, depolymerization, crosslinking, and changes in hydrogen bonding [13–15]. In starch-based materials, such mechanisms may modify surface roughness, hydrophilicity, water absorption, swelling capacity, pasting behavior, thermal stability, and short- or long-range molecular order without necessarily destroying the native crystalline pattern. However, the direction and magnitude of these changes depend strongly on plasma conditions, including treatment time, discharge power, voltage, working gas, and the botanical origin of the starch [13–15].

From a technological perspective, rice quality is strongly influenced by the structural behavior of starch and storage proteins, particularly amylose content, crystalline organization, gelatinization behavior, pasting properties, retrogradation tendency, and the integrity of the starch-protein matrix. These parameters determine water absorption during cooking, MCT, SL, cooked rice texture, and final consumer acceptance [16,17]. Paddy husking and polishing may also affect these properties by imposing friction, pressure, and abrasion on the grain surface, removing bran and aleurone layers, creating cracks or microcracks, and changing water access to the starch-protein matrix [16,18–21]. Accordingly, this study was designed to evaluate the effect of ACP treatment on the technological, structural, thermal, and macromolecular properties of *local Tarom* rice, with emphasis on rice starch and glutelin, and to compare its effects with those of parboiling and untreated control samples.

Materials and methods

Materials

Local Tarom paddy rice (3 kg) was obtained from Dehestan Rice Processing Company (Mazandaran, Iran). After procurement, the grains were cleaned to remove physical impurities, packed in polyethylene bags, transferred to the Food Science and Technology Laboratory, and stored at room temperature until treatment. The samples were weighed and divided into 0.5 kg portions. Distilled/deionized water was used for soaking, washing, cooking tests, sample preparation, and instrumental analyses. Ultrapure nitric acid used for heavy-metal digestion was purchased from Merck (Darmstadt, Germany). Iodine, potassium iodide, sodium hydroxide, and phosphoric acid used for amylose determination and protein extraction were of analytical grade and supplied by Merck (Darmstadt, Germany) and Sigma–Aldrich (St. Louis, MO, USA). All other chemicals and reagents used in this study were of analytical grade. The main instruments used for sample characterization included an atomic force microscope, model NVB100 (Olympus, Tokyo, Japan), equipped with a NanoScope IIIa controller (Digital Instruments, Santa Barbara, CA, USA), a Chirascan V100 circular dichroism spectrometer (Applied Photophysics, UK), a UV–Visible spectrophotometer, model 722 G (Renonlab, China). General laboratory equipment, including a hot-air oven, boiling water bath, analytical balance, desiccator, sieve, centrifuge, aluminum pans, Falcon tubes,

and standard glassware, was used for moisture determination, cooking tests, sample digestion, thermal analysis, and sample preparation.

Rice treatment

Atmospheric cold plasma treatment

ACP treatment was generated using a dielectric barrier discharge system with an input voltage of 12 kV, frequency of 10 kHz, and power of 200 W. A polypropylene pad was placed as the dielectric barrier at the top and bottom of the container to improve discharge uniformity. Paddy samples were exposed to air plasma for 30, 60, 90, and 120 s and were coded as F1, F2, F3, and F4, respectively. The parboiled sample and control sample were coded as F5 and F6, respectively. Approximately 500 g of rice was used for each treatment. The samples were placed in a uniform layer to ensure comparable exposure of all grains to the plasma discharge. Because ACP is a non-thermal process, the treatment was designed to minimize appreciable temperature increase. Therefore, the observed modifications were mainly attributed to the physical and chemical effects of plasma-generated reactive species rather than direct heating.

Parboiling

The paddy was divided between two 1-L beakers, with 500 g in each beaker. Distilled water was added to the 1-L mark. The paddy was washed repeatedly, with the water replaced until it remained clear. The beakers were placed in a water bath and heated to 65°C, as monitored with a mercury thermometer. The samples were soaked at 65°C for 5 h, drained, spread evenly in an aluminum tray, and steamed in a covered water bath at 100°C for 10 min. The parboiled samples were then air-dried for 2–3 d until the moisture content reached 11–13% (wet basis) [22].

Dry paddy husking and polishing

ACP-treated rice samples were prepared using a dry method and through conventional rice husking and bleaching. In this method, first, paddy (rice in husk) was directly subjected to the husking process without any heat treatment or initial soaking. For this purpose, the paddy was cleaned, if necessary, in terms of size uniformity and removal of physical impurities (such as pebbles, straw and chaff, broken grains and weed seeds) with the help of sieve and blower and then transferred to a mechanical huller. In the paddy husking stage, the outer husk was separated only by applying mechanical force (friction and pressure), and by properly adjusting the distance between the rollers and the intensity of the force, the hard husk of the grain was separated and the BR product was obtained, in a way that minimal damage and breakage was caused to the grains. The resulting brown rice, after passing through a fan or vibrating sieve, was refined to remove remaining husks and light impurities. Next, in order to produce conventional WR, the bleaching (polishing) stage was performed on the BR. For this purpose, the cleaned BR was

directed to the bleaching machine and, using controlled friction force, the bran layer and part of the aleurone layer were separated from the surface of the grains. The operating conditions of the machine (duration of passage, pressure applied to the grains and intensity of friction) were adjusted in such a way that the degree of whitening of the rice was within the normal consumption range and excessive breakage of the grains was prevented. If necessary, the bleaching process was carried out in one or two successive stages with milder intensities to achieve the desired whiteness. Finally, the produced white rice was again passed through a sieve and fan to remove broken grains, dust and remaining bran particles and to obtain a uniform and standard sample as a dry control sample. This sample did not undergo any heat treatment, soaking or gelatinization and was subjected to only dry mechanical processes (paddy dehusking and bleaching). Subsequently, all ACP, control and parboiling treatments were performed using this paddy dehusking method [23]. Then, the ACP-treated rice samples were milled using a laboratory-scale machine at Mazra Khoshe Talaei Kabudwal Company (Dawlatabadi Rice Mill). The control sample was also milled using the dry method. The rice grains were polished using an experimental friction rice mill to achieve a milling efficiency (yield after polishing) of 90–91%. Then, in order to perform some analyses, the white rice produced was converted into flour using a cyclone mill and flour with a uniform particle size (diameter 1 mm) was used.

Sample characterization

The analytical methods in this section were arranged to follow the same order used in the Results and Discussion section: moisture content (MC), cooking properties, Fourier transform infrared spectroscopy (FTIR), X-ray diffraction (XRD), atomic force microscopy (AFM), color analysis, differential scanning calorimetry (DSC), and circular dichroism (CD). This organization provides a logical sequence from basic compositional stability to cooking behavior, chemical structure, crystalline order, surface morphology, color quality, thermal behavior, and protein conformation.

Moisture content

The moisture content of the treated samples was determined according to AOAC Official Method 925.10 (AOAC, 2000). Approximately 5 g of each sample was dried at 105°C for 3 h, cooled in a desiccator to prevent moisture reabsorption, and weighed. Moisture content was calculated using Eq. (1):

$$\text{Moisture (\%)} = [(W_1 - W_2) / W_1] \times 100$$

W_1 = initial sample mass (g)

W_2 = sample mass after drying (g)

Cooking properties

Cooking properties were evaluated as minimum cooking time (MCT), water absorption index (WAI), and solid loss (SL), as described below [24,25].

Minimum cooking time (MCT)

A 15 g portion of rice grains was placed in six beakers containing 10 mL of boiling distilled water in a boiling water bath. The grains were cooked until the opaque center disappeared completely and the required time was recorded as MCT in s.

Water absorption index (WAI)

A 1 g portion of rice was mixed with 10 mL of distilled water in a test tube and heated in a boiling-water bath for 25 min. After cooking, the contents were transferred to a preweighed sieve and allowed to drain for 10 min. The cooked and drained grains were weighed. The measurement was performed in triplicate, and WAI was calculated using Eq. (2):

WAI (g/g) = mass of cooked rice (g) / mass of uncooked rice (g)

Solid loss (SL)

The drained cooking water was collected and dried in a hot-air oven at 105°C for 12 h. After the residue reached a constant mass, it was cooled in a desiccator and weighed. Solid loss was calculated using Eq. (3):

SL (%) = [mass of residue in cooking water (g) / mass of uncooked rice (g)] × 100

Fourier-transform infrared spectroscopy

FTIR spectroscopy equipped with an attenuated total reflectance (ATR) module was employed for chemical characterization. For this purpose, milled rice samples were placed directly onto the ATR crystal without pellet preparation to ensure complete contact between the sample and the crystal surface. Spectra were collected within the wavenumber range of 4000–400 cm^{-1} with a spectral resolution of 4 cm^{-1} using 36 scans. To evaluate the degree of structural order in starch, the absorbance intensity ratio of the bands at 1047 and 1022 cm^{-1} was calculated as an index of short-range order, indicating the relative crystallinity of the crystalline domains in the starch structure. The calculation was performed following the method reported in Reference [5]. Finally, the obtained spectra were used for identification of functional groups and assessment of chemical changes in the samples.

X-ray diffraction analysis

To investigate the changes in the crystal structure of treated samples, they were analyzed under conditions of 40 kV and 40 mA using Cu Kα radiation (λ = 0.154 nm). Diffraction angles from 5° to 40° (2θ) were collected with a scan increment of 0.0205° and a scan rate of 2°/min. The relative crystallinity

(RC) of the samples, which is the amount of crystalline material compared to the non-crystalline material, was then calculated [5].

Atomic force microscopy

To examine the surface and structural changes of rice starch granules, an atomic force microscope (AFM) model NVB100 (Olympus, Tokyo, Japan) with a NanoScope IIIa controller (Digital Instruments, Santa Barbara, CA, USA) was used. The samples were placed on a mica surface and tested at ambient temperature (25°C) and relative humidity. Imaging was performed in Tapping Mode™ with a resonant frequency of approximately 300 kHz. The scan dimensions varied between 500 × 500 nm and 10 × 10 μm, and the scan frequency ranged from 0.1 to 1 Hz. This method allowed the observation of nanoscale structures on the starch surface in conditions close to the natural state. This test was performed in triplicate [6].

Color analysis

Color analysis was performed using a HunterLab colorimeter after calibration with the standard white and black tiles supplied by the manufacturer. The rice samples were placed in a sample cup to obtain a uniform and flat surface, and color parameters were recorded in the CIE L*, a*, and b* system, where L* indicates lightness, a* represents the red-green axis, and b* represents the yellow-blue axis. Measurements were carried out in triplicate for each sample, and the average values were reported [26].

Differential scanning calorimetry

Differential scanning calorimetry (DSC) was performed according to Dang et al. (2023), with minor modifications [4]. Rice flour (3 mg) and deionized water (9 μL) were placed in an aluminum pan, which was immediately sealed. The sealed samples were equilibrated at room temperature for 24 h, and an empty sealed pan was used as the reference. Samples were heated from 20 to 120°C at 0.083°C s^{-1}. The onset temperature of gelatinization (To), conclusion temperature (Tc), and gelatinization enthalpy (ΔH, J g^{-1}) were obtained from the thermograms using STARe software.

Circular dichroism spectroscopy

Circular dichroism (CD) spectroscopy was performed according to Yang et al. (2025), with minor modifications [27]. Glutelin was extracted from defatted rice flour using 0.1 mol L^{-1} NaOH. Flour (1 g) was suspended in the alkaline solution, stirred for 1 h, and centrifuged at 10,000 rpm for 15 min. The supernatant was collected and adjusted to pH 7.0–7.2 with dilute phosphoric acid. CD spectra were recorded using a Chirascan V100 spectrometer (Applied Photophysics, UK) over 176–260 nm. The final protein concentration was 0.1 g L^{-1}, and both the bandwidth and step size were 1 nm. The proportions of α-helix, β-sheet, turn, and unordered structure were estimated using CDPro software.

Statistics and reproducibility

Data are presented as mean ± standard deviation (SD). Statistical analyses were performed using SPSS version 26.0. Group means were compared using one-way analysis of variance followed by a post hoc

multiple-comparison test when the omnibus test was significant. All tests were two-sided, and the significance level was set at α = 0.05.

Results and discussion

Moisture content

The moisture content (MC) of the rice samples ranged from 8.814 ± 0.643 to 9.673 ± 0.291% (w/w), as shown in Table 1. No significant difference was observed among ACP-treated, parboiled, and control samples ($p > 0.05$). In the ACP-treated samples, the absence of significant MC changes can be attributed to the non-thermal nature and short exposure time of the process, because plasma-generated reactive species mainly interact with the grain surface under the applied conditions. However, ACP may still affect water contact angle, surface energy, hydration rate, and cooking behavior without markedly changing bulk moisture content [8,28,29]. Similar results have been reported by Cao et al. (2024) in CP-treated rice, such that repeated helium CP treatments improved water contact angle, water absorption rate, and cooking behavior while preserving the general hygroscopic characteristics of rice [28]. On the other hand, in the parboiling process, although the water absorption rate increases during the soaking and steaming stages, the final drying stage leads to a decrease and stabilization of the grain moisture content within the appropriate storage range [30–32]. This interpretation is also consistent with parboiling studies showing that soaking and steaming strongly affect water uptake and gelatinization, whereas drying controls the final moisture and storage stability of the product [27,33]. These MC results therefore provide the baseline for the subsequent cooking analysis, because they confirm that any changes in MCT, WAI, or SL should mainly be interpreted as treatment-induced effects rather than consequences of different initial moisture levels.

Table 1
Water absorption behavior of treated samples.

Parameters	Samples					
	F_1	F_2	F_3	F_4	F_5	F_6
Moisture	8.814 ± 0.643 [a]	9.673 ± 0.291 [a]	9.411 ± 0.470 [a]	9.340 ± 0.533 [a]	9.141 ± 0.463 [a]	9.255 ± 0.041 [a]
Cooking properties						
Minimum Cooking Time (s)	1517.643 ± 63.344 [b]	1455.677 ± 35.866 [b]	1352.753 ± 30.692 [c]	1635.817 ± 5.046 [a]	1662.083 ± 7.839 [a]	1538.083 ± 16.660 [b]
Water Absorption Index (g/g)	2.196 ± 0.397 [a]	2.272 ± 0.238 [a]	2.281 ± 0.352 [a]	2.400 ± 0.143 [a]	2.381 ± 0.258 [a]	2.358 ± 0.224 [a]
Solid Loss (g/g)	0.021 ± 0.013 [a]	0.020 ± 0.004 [a]	0.020 ± 0.007 [a]	0.022 ± 0.012 [a]	0.013 ± 0.001 [a]	0.022 ± 0.013 [a]
* Samples are reported as atmospheric cold plasma treated at 30s (F_1), 60s (F_2), 90s (F_3), 120s (F_4), parboiled samples (F_5) and control sample (F_6).						
** Values are reported as Mean ± Standard Deviation (SD).						
*** Samples with different letter in each raw is considered as significant difference ($p \leq 0.05$).						

Cooking properties

Cooking properties were determined by parameters, including Minimum Cooking Time (MCT), Water Absorption Index (WAI), and Solid Loss (SL). Together, these indices describe the cooking efficiency, water interaction capacity, and structural stability of rice grains during hydration and heating. Since no significant differences ($p > 0.05$) were observed in the initial MC of the samples, the changes in MCT can be more confidently attributed to treatment-induced changes in grain structure, surface accessibility, and water diffusion rather than to differences in initial water level. MCT, as a key indicator of rice cooking behavior, reflects the time required for the kernel to become fully cooked and is affected by starch organization, gelatinization behavior, grain permeability, and starch-protein interactions [34]. According to Table 1, MCT ranged from 1352.753 ± 30.692 to 1662.083 ± 7.839 s. The lowest value was observed in F3 (i.e., ACP-treated sample for 90 s), while the highest value was observed in F5 (i.e., parboiled sample). Among ACP-treated samples, MCT decreased from F1 (i.e., ACP-treated sample for 30 s) to F3, suggesting that short-to-moderate ACP exposure facilitated cooking. Similar results were reported by Thirumdas et al. (2015), who observed that low-temperature plasma treatment improved the cooking quality of basmati rice by modifying surface characteristics and water interaction behavior [35]. This finding is also consistent with Liu et al. (2021), who reported that cold plasma treatment reduced the cooking time of Chinese milled rice and changed its surface structural properties [29]. Cao et al. (2024)

also found that repeated CP treatment decreased the water contact angle and cooking time of rice, indicating improved water accessibility at the grain surface [28]. However, increasing ACP exposure to 120 s in F4 reversed this decreasing trend, indicating that the effect of ACP on cooking behavior was not simply proportional to exposure time. At prolonged exposure, surface rearrangement or modification of the starch-protein matrix may have partially restricted efficient water penetration. In contrast, the increased MCT of F5 may be related to starch gelatinization during soaking/steaming followed by drying-induced matrix densification and retrogradation, which can limit water migration during subsequent cooking [33].

Although ACP treatment significantly affected MCT, neither WAI nor SL showed significant differences among the samples ($p > 0.05$). This finding suggests that the reduction in cooking time, particularly in F3, was not associated with increased water-holding capacity or excessive leaching of soluble components during cooking. Therefore, the improved cooking behavior could not be fully explained by conventional hydration-related parameters alone. This result is supported by Thirumdas et al. (2016), who showed that plasma-treated brown rice can exhibit improved cooking and textural properties without necessarily producing severe grain disintegration [36]. Similarly, Noppakun et al. (2021) reported that plasma treatment altered cooking and physical qualities of pigmented rice, suggesting that plasma-induced surface modification can improve cooking behavior while maintaining grain integrity [37]. These observations highlighted the need for further investigation of structural and molecular changes induced by ACP treatment. Accordingly, FTIR spectroscopy was performed to determine whether modifications in starch-related functional groups or short-range molecular interactions contributed to the observed reduction in MCT.

FTIR spectroscopy

FTIR spectroscopy was interpreted based on the main starch-related absorption bands, particularly O-H stretching, C-H stretching, bound-water-associated vibrations, and the fingerprint region related to C-O and glycosidic bond vibrations. These bands were used to assess whether ACP and parboiling treatments altered the main chemical structure or only induced limited short-range molecular modifications. FTIR spectra of all samples were monitored in the range of 4000–400 cm^{-1}. As shown in Fig. 1, all samples showed the characteristic starch-related bands at approximately 3288, 2925, 1644, and 995 cm^{-1}. The absence of new peaks and the preservation of the main bands indicate that neither ACP nor parboiling generated new dominant functional groups under the applied conditions. However, changes in band intensity were observed, suggesting limited molecular rearrangement and surface modification. Similar findings were reported by Thirumdas et al. (2016) and Pal et al. (2016), who found that plasma treatment changed the intensity of starch- and protein-related FTIR bands in rice flour without indicating complete destruction of the main carbohydrate backbone [38,39]. This finding is also consistent with Chaple et al. (2020), who observed that ACP treatment changed wheat flour hydration and functionality while FTIR mainly reflected modifications in bonding environment rather than formation of entirely new chemical structures [40]. The broad band near 3288 cm^{-1}, assigned to O-H stretching, changed with ACP exposure time and may indicate altered hydrogen bonding or increased surface

polarity due to plasma-generated reactive species [41]. The band at 2925 cm^{-1}, related to C-H stretching, showed limited change, indicating that the carbohydrate backbone was not severely degraded [42]. The band near 1644 cm^{-1}, associated with bound water, varied among treatments, probably reflecting changes in water-starch interactions after surface activation [41,43,44]. The fingerprint region around 995 cm^{-1}, associated with C-O and glycosidic bond vibrations, showed intensity changes that may be related to limited rearrangement of starch chains without destruction of the main polysaccharide structure [40]. Overall, FTIR confirmed that ACP mainly caused controlled surface or short-range molecular modifications rather than complete chemical disruption. The FTIR results therefore confirm the cooking data by suggesting that faster cooking was not caused by severe chemical degradation of starch. However, FTIR mainly reflects functional groups and short-range molecular interactions; therefore, XRD was required next to determine whether the long-range crystalline organization of rice starch was preserved or modified after ACP and parboiling.

X-ray diffraction

The XRD analysis was evaluated using diffraction peak position, crystalline pattern, relative crystallinity, mean full width at half maximum (FWHM), and apparent crystallite size. These parameters collectively describe the long-range order of rice starch and help clarify whether ACP altered starch crystallinity or mainly affected the grain surface. XRD analysis was performed to evaluate the effect of ACP and parboiling treatments on the long-range crystalline structure of rice starch. The XRD patterns of all samples showed characteristic diffraction peaks around 15°, 17–18°, and 23° 2θ, indicating that the typical A-type crystalline pattern of cereal starch was retained after both ACP and parboiling treatments [41,45–48]. The changes in the molecular structure of rice starch after plasma treatment are presented in Fig. 2. Similar results have been reported by Thirumdas et al. (2015) and Cao et al. (2024), who observed that CP treatment improved rice cooking or functional behavior while preserving the main crystalline pattern or short-range molecular order of rice starch [28,48]. This result is also consistent with Zhou et al. (2018), who reported that atmospheric-pressure plasma did not change the crystalline type of maize starch, although relative crystallinity and short-range order were slightly modified [48]. The absence of new peaks and the lack of major peak shifts indicate that none of the treatments induced the formation of a new crystalline polymorph. Therefore, the main crystalline framework of rice starch was largely preserved, and the differences among samples were mainly related to changes in peak intensity, peak broadening, relative crystallinity, and apparent crystallite size. According to Table 2, relative crystallinity ranged from 24.91% in F6 (i.e., control sample) to 27.49% in F1 (i.e., ACP-treated sample for 30 s). Among ACP-treated samples, F1, F2 (i.e., ACP-treated sample for 60 s), F3 (i.e., ACP-treated sample for 90 s), and F4 (i.e., ACP-treated sample for 120 s) showed relative crystallinity values of 27.49, 26.63, 26.25, and 26.63%, respectively. These values indicate only slight changes compared with F6 and suggest that ACP treatment did not cause extensive disruption of starch crystallites. In contrast, parboiling studies have shown that more severe hydrothermal conditions can reduce crystallinity through starch gelatinization and molecular rearrangement [49–51]. Therefore, the relatively preserved crystallinity in ACP-treated samples supports the view that ACP produced milder structural modification than

conventional hydrothermal processing. F3 showed 26.25% relative crystallinity, 1.23° mean FWHM, and 6.91 nm mean crystallite size, indicating that ACP treatment caused only limited changes in the crystalline structure of starch. Therefore, the relationship between the XRD parameters and the reduced MCT of F3 should be interpreted together with the AFM results in the following section.

Table 2
Quantitative XRD parameters of treated rice samples.

Parameters	Samples					
	F_1	F_2	F_3	F_4	F_5	F_6
Crystal type	A-type	A-type	A-type	A-type	A-type	A-type
Relative crystallinity (%)	27.49	26.63	26.25	26.63	25.96	24.91
Mean FWHM (°)	1.27	1.20	1.23	1.28	1.23	1.20
Mean crystallite size D (nm)	6.71	7.20	6.91	6.65	7.04	7.09
Highest peak	17–18° doublet	17–18° doublet	17–18° doublet	17–18° doublet	17–18° doublet	17–18° doublet

* Samples are reported as atmospheric cold plasma treated at 30s (F_1), 60s (F_2), 90s (F_3), 120s (F_4), parboiled samples (F_5) and control sample (F_6).

Atomic force microscopy

The AFM interpretation was based on five surface topography parameters: mean surface height, RMS roughness, average roughness, surface skewness, and excess kurtosis. These parameters provide complementary information on surface elevation, roughness intensity, roughness distribution, surface asymmetry, and the presence or absence of sharp localized defects. AFM was used to evaluate nanoscale changes in the surface morphology of rice grains after ACP and parboiling treatments. The five AFM parameters collectively indicated that ACP treatment modified the surface topography in a treatment-time-dependent manner. Visual inspection of the AFM images (Fig. 3) revealed clear differences in surface topography among the investigated samples. F1, F2, F4, F5, and F6 exhibited irregular surfaces with various elevations and depressions distributed across the scanned area. In contrast, F3 displayed a markedly different morphology characterized by pronounced ridge-like structures and greater height variations, indicating substantial surface reorganization after ACP treatment. These topographical features suggest that ACP exposure modified the external surface of rice grains, generating localized protrusions and depressions that increased surface heterogeneity. The distinct morphology observed in F3 was consistent with its higher roughness-related parameters reported in Table 3. According to Table 3, mean surface height of investigated samples ranged from 29.891 ± 7.005 to 192.207 ± 77.300 nm, RMS roughness ranged from 10.477 ± 2.520 to 65.624 ± 18.590 nm, and average roughness ranged from 8.015 ± 1.829 to 52.278 ± 12.305 nm. Among all samples, F3 (i.e., ACP-treated sample for 90 s) showed the highest mean surface height, RMS roughness, and

average roughness, indicating the most pronounced surface modification (as demonstrated in Fig. 3). Similar results have been reported for plasma-modified starches and microparticles, where reactive plasma species caused surface etching, roughness development, and nanoscale surface reorganization without complete bulk destruction [39,42,52–55]. This finding is consistent with Ayoub et al. (2006), who used AFM to show that disordering processes on rice starch granule surfaces can be detected as nanoscale changes in surface features [56]. The AFM response was consistent with the MCT results, because F3 also showed the shortest cooking time. Therefore, moderate ACP exposure probably improved water accessibility by modifying the external surface of the grain. However, this modification did not cause severe structural damage, because WAI and SL did not differ significantly among samples and XRD retained the A-type crystalline structure. Surface skewness further showed that ACP changed the symmetry of the surface height distribution. Negative skewness in F3 and F4 suggests a greater contribution of pits or depressions, whereas positive skewness in F2 indicates a surface dominated by protrusions or ridges [55,57–61]. This behavior confirms that the ACP effect was not linear with exposure time. In contrast, excess kurtosis did not differ significantly among samples ($p > 0.05$), indicating that ACP did not generate extremely sharp peaks or severe localized defects. Based on these findings, AFM supports the conclusion that ACP mainly produced controlled and surface-oriented modifications rather than destructive changes in the rice grain matrix. The AFM findings validate the interpretation derived from cooking properties, FTIR, and XRD by showing that the main ACP effect was concentrated on the grain surface rather than within the bulk crystalline matrix. Because changes in surface roughness and topography can also influence light scattering and visual appearance, color analysis was required to determine whether these surface modifications produced quality-relevant color changes.

Table 3
AFM results of treated rice samples.

Parameters	Samples					
	F_1	F_2	F_3	F_4	F_5	F_6
Mean Surface Height (nm)	75.962 ± 20.550 b	29.891 ± 7.005 c	192.207 ± 77.300 a	63.793 ± 6.200 b	43.766 ± 3.250 bc	72.189 ± 8.000 b
RMS Roughness (nm)	23.067 ± 5.255 b	10.477 ± 2.520 b	65.624 ± 18.590 a	15.043 ± 0.142 b	16.311 ± 3.085 b	20.810 ± 5.205 b
Average Roughness (nm)	17.913 ± 3.620 b	8.015 ± 1.829 b	52.278 ± 12.305 a	11.991 ± 0.181 b	13.038 ± 2.780 b	16.699 ± 4.830 b
Surface Skewness	0.039 ± 0.133 bc	0.631 ± 0.149 a	(−0.175) ± 0.105 c	(−0.084) ± 0.140 c	0.318 ± 0.012 b	(−0.025) ± 0.182 c
Excess Kurtosis	0.412 ± 0.320 a	1.541 ± 0.548 a	(−0.206) ± 0.747 a	0.089 ± 0.246 a	0.582 ± 0.313 a	0.370 ± 0.782 a

* Samples are reported as atmospheric cold plasma treated at 30s (F_1), 60s (F_2), 90s (F_3), 120s (F_4), parboiled samples (F_5) and control sample (F_6).

** Values are reported as Mean ± Standard Deviation (SD).

*** Samples with different letter in each raw is considered as significant difference ($p \leq 0.05$).

**** Surface skewness and over-skewedness are dimensionless parameters. Since their mean values were close to zero and some were negative, the standard deviation (SD) in some samples could exceed the absolute mean. Therefore, these parameters were interpreted with caution, with the emphasis on statistically significant differences and trends in the overall surface distribution rather than absolute numerical magnitude.

Color analysis

Color analysis was done to compare ACP-induced surface color changes with hydrothermal color changes caused by parboiling. It was monitored by CIE L*, a*, b*, and total color difference (ΔE) parameters, which describe lightness, red-green tendency, yellow-blue tendency, and the overall magnitude of color change, respectively. According to Table 4, L* values ranged from 72.690 ± 0.040 to 76.920 ± 0.060, a* ranged from 0.336 ± 0.005 to 1.093 ± 0.028, b* ranged from 16.566 ± 1.752 to 23.606 ± 0.015, and ΔE ranged from 0.020 ± 0.000 to 0.056 ± 0.005. As declared, F6 (i.e., control sample) showed the highest L* value, whereas F5 (i.e., parboiled sample) showed the lowest L* and the highest a*, b*, and ΔE values. This confirms that parboiling caused the most pronounced darkening, reddening, and yellowing of the rice samples. Similar results have been reported by Lamberts et al. (2006), who showed that color changes in parboiled rice are strongly associated with browning reactions and bran pigment migration during hydrothermal processing [62,63]. Bhattacharya (1996) also reported that rice color changes during parboiling follow processing-dependent browning kinetics, supporting the higher

a*, b*, and ΔE values observed in F5 [64]. In contrast, ACP-treated samples generally showed milder color deviations than F5, suggesting that ACP-induced color changes were mainly related to surface oxidation, surface roughness, and altered light reflection rather than extensive thermal browning [29,65,66]. Similar mild color responses after cold plasma have been reported in brown rice studies, where plasma treatment improved microbial or physicochemical quality with limited changes in visual quality compared with thermal treatments [65,66]. The color results are also consistent with AFM observations, because plasma-induced surface modification may influence light scattering and reflectance. However, color changes did not follow a simple linear trend with treatment time, indicating that the visual response depended on the balance between surface etching, oxidation, and roughness development. Overall, compared with parboiling, ACP had a less severe effect on rice color while still producing functional surface modifications. The color results complement the AFM findings by indicating that ACP-induced surface modification affected visual quality less severely than parboiling. However, color and surface morphology do not directly describe molecular mobility or heat resistance; therefore, DSC analysis was required to evaluate whether the structural modifications observed by XRD and AFM were accompanied by changes in the thermal behavior of rice starch-related macromolecular structures.

Table 4
Color analysis of treated rice samples.

Parameters	**Samples**					
	F_1	**F_2**	**F_3**	**F_4**	**F_5**	**F_6**
L*	74.623 ± 0.051 ^{d}	74.853 ± 0.090 ^{c}	75.306 ± 0.020 ^{b}	73.513 ± 0.096 ^{e}	72.690 ± 0.040 ^{f}	76.920 ± 0.060 ^{a}
a*	0.510 ± 0.030 ^{c}	0.366 ± 0.005 ^{d}	0.366 ± 0.015 ^{d}	0.636 ± 0.028 ^{b}	1.093 ± 0.028 ^{a}	0.336 ± 0.005 ^{d}
b*	17.850 ± 0.045 ^{b}	18.866 ± 0.051 ^{b}	19.090 ± 0.026 ^{b}	16.566 ± 1.752 ^{b}	23.606 ± 0.015 ^{a}	18.056 ± 0.015 ^{b}
AB (ΔE)	0.030 ± 0.000 ^{c}	0.020 ± 0.000 ^{d}	0.020 ± 0.000 ^{d}	0.040 ± 0.000 ^{b}	0.056 ± 0.005 ^{a}	0.020 ± 0.000 ^{d}
* Samples are reported as atmospheric cold plasma treated at 30s (F_1), 60s (F_2), 90s (F_3), 120s (F_4), parboiled samples (F_5) and control sample (F_6).						
** Values are reported as Mean ± Standard Deviation (SD).						
*** Samples with different letter in each raw is considered as significant difference ($p \leq 0.05$).						

Differential scanning calorimetry

DSC analysis was interpreted using crystallization temperature (Tc), glass transition temperature (Tg), melting temperature (Tm), and the thermal transition range (ΔT = Tm − Tg). These parameters were

considered together to evaluate treatment-induced changes in molecular mobility, thermal rearrangement, melting resistance, and the apparent thermal stability of rice starch-related structures. DSC was used to evaluate treatment-induced changes in the thermal behavior of rice macromolecules. The values of Tc, Tg, Tm, and ΔT ranged from 82.9 ± 0.3 to 133.8 ± 0.6°C, 50.7 ± 0.2 to 67.5 ± 0.4°C, 160.3 ± 0.5 to 193.9 ± 0.7°C, and 96.9 ± 0.5 to 141.2 ± 0.7°C, respectively (Table 5). The highest Tc value was observed in F2 (i.e., ACP-treated sample for 60 s), which may indicate an increased tendency of starch chains to rearrange and form more ordered regions after mild plasma exposure. In contrast, the lowest Tc was observed in F5 (i.e., parboiled sample), probably because hydrothermal treatment caused gelatinization and partial disruption of native crystalline regions [33]. Similar DSC behavior has been reported in plasma-treated starch systems, where cold plasma caused changes in gelatinization or transition parameters without necessarily destroying the entire crystalline structure [45,47,67,68]. This finding is also consistent with Thirumdas et al. (2016), who reported reduced peak gelatinization temperature after plasma treatment of basmati rice flour, indicating plasma-induced modification of starch thermal behavior [39]. In terms of Tg, F1 (i.e., ACP-treated sample for 30 s) showed the highest value, suggesting reduced mobility of amorphous chains after short ACP exposure. However, Tg decreased at intermediate treatment times and then increased again in F4 (i.e., ACP-treated sample for 120 s), indicating a non-linear thermal response through ACP treatment. The most notable result was observed in F3 (i.e., ACP-treated sample for 90 s), which showed the highest Tm (193.9 ± 0.7°C) and ΔT (141.2 ± 0.7°C). This suggests that F3 had the highest apparent thermal stability among the samples. The improved thermal behavior of F3 was consistent with the AFM and XRD results: ACP treatment at 90 s markedly modified surface morphology while preserving the A-type crystalline pattern. On the other hand, parboiling-related studies have shown that hydrothermal processing can decrease crystallinity and modify DSC endotherms due to starch gelatinization and amylose-lipid interactions [49–51]. Therefore, the DSC differences between ACP and F5 support the conclusion that ACP caused controlled molecular rearrangement, whereas parboiling caused stronger hydrothermal modification. In summary, DSC confirmed that ACP treatment, particularly at 90 s, improved the thermal resistance of rice starch-related structures without severe destruction of the crystalline framework. These DSC results support the previous XRD data, because the increased thermal resistance of F3 occurred while the A-type crystalline pattern was preserved, suggesting controlled molecular rearrangement rather than crystalline destruction. Since DSC mainly reflects thermal transitions of starch-related structures and does not directly describe protein conformation, CD spectroscopy was necessary to determine whether ACP also affected the secondary structure of rice glutelin.

Table 5
DSC results of treated rice samples.

Parameters	Samples					
	F_1	F_2	F_3	F_4	F_5	F_6
Tc (°C)	102.8 ± 0.3 [e]	133.8 ± 0.6 [a]	129.1 ± 0.4 [b]	119.1 ± 0.5 [d]	82.9 ± 0.3 [f]	121.6 ± 0.4 [c]
Tg (°C)	67.5 ± 0.4 [a]	59.7 ± 0.3 [c]	52.7 ± 0.3 [e]	62.5 ± 0.4 [b]	50.7 ± 0.2 [f]	58.7 ± 0.3 [d]
Tm (°C)	164.4 ± 0.5 [e]	190.6 ± 0.7 [c]	193.9 ± 0.7 [a]	192.9 ± 0.7 [b]	160.3 ± 0.5 [f]	177.9 ± 0.5 [d]
ΔT = Tm – Tg (°C)	96.9 ± 0.5 [e]	130.9 ± 0.6 [b]	141.2 ± 0.7 [a]	130.4 ± 0.6 [b]	109.6 ± 0.5 [d]	119.2 ± 0.7 [c]
* Samples are reported as atmospheric cold plasma treated at 30s (F_1), 60s (F_2), 90s (F_3), 120s (F_4), parboiled samples (F_5) and control sample (F_6).						
** Values are reported as Mean ± Standard Deviation (SD).						
*** Samples with different letter in each raw is considered as significant difference ($p \leq 0.05$).						

Circular dichroism analysis

CD spectroscopy in the far-UV region was used to evaluate the secondary structure of rice glutelin under ACP and parboiling treatments. In protein CD analysis, the far-UV region mainly reflects electronic transitions of peptide bonds and is commonly used to estimate secondary structural elements, including α-helix, β-sheet, turns, and unordered structures. α-helical proteins generally show two negative bands near 208 and 222 nm, whereas β-sheet-rich proteins usually show a negative band close to 216–218 nm and a positive band near 195 nm [69]. As shown in Fig. 4, the CD spectra of F1–F6 showed some fluctuations in ellipticity intensity and curve shape, especially around 213, 218, and 232 nm. However, the quantitative secondary structure data presented in Table 6 were almost unchanged among the treatments. The α-helix content was 11.50% in all samples. The β-sheet content was 31.20% in all samples, except F3, which showed 31.10%. The turn and other structural fractions remained constant at 14.90% and 42.40%, respectively. Therefore, the 0.10 percentage-unit difference in β-sheet content in F3 was too small to be interpreted as a real conformational change, particularly because it was not accompanied by standard deviation, statistical separation, or coordinated changes in the other secondary structure components. The results indicate that ACP treatment for 30–120 s and parboiling did not cause a detectable change in the secondary structure composition of rice glutelin. This finding suggests that glutelin remained conformationally stable under the applied treatment conditions. Quddus and Ma (2003) reported that rice glutelin contains a considerable proportion of β-form and random coil structures and that CD spectroscopy can detect glutelin conformational changes under stronger perturbing conditions, such as changes in pH, salts, sodium dodecyl sulfate, and ethylene glycol [70]. In

the present study, the unchanged α-helix, β-sheet, turn, and other structural fractions suggest that the applied ACP and parboiling conditions were not sufficient to induce measurable unfolding or rearrangement of rice glutelin. This interpretation agrees with Held et al. (2019), who observed that radio-frequency CP treatment did not significantly change protein aggregation or secondary structure in hard wheat flour, although some flour and dough properties were modified [71]. Their findings show that cold plasma can affect cereal systems without necessarily causing measurable changes in protein secondary structure, depending on the matrix and processing conditions. Warne et al. (2021) also reported that proteins are more strongly affected by cold plasma at higher intensities and longer treatment times, while lower power levels and shorter treatments may have limited effects on food biomolecules [72]. Similarly, Olatunde et al. (2023) emphasized that plasma-induced protein modification depends on treatment time, gas composition, discharge power, sample state, and accessibility of reactive species to the protein molecules [73]. The stability of glutelin secondary structure in the present study can therefore be attributed mainly to the treatment mode and limited accessibility of plasma-generated reactive species to the internal protein matrix. ACP was applied to intact rice grains rather than to extracted glutelin or a protein solution. Consequently, reactive species probably interacted mainly with the grain surface and outer starch-rich regions, while glutelin embedded within the internal starch-protein matrix was less exposed. The relatively short treatment times of 30–120 s may also explain why surface-related properties were modified while the secondary structure of glutelin remained unchanged. In general, CD analysis showed that the spectral curves had minor fluctuations in ellipticity intensity, but these fluctuations were not reflected in the calculated secondary structure composition. Therefore, the CD results should be interpreted as evidence of glutelin structural stability rather than protein denaturation. The improved cooking behavior of F3 was consequently more closely related to surface-oriented ACP effects, including surface etching, increased roughness, and improved water accessibility, rather than changes in glutelin conformation. This interpretation is consistent with the AFM results and with the preservation of the A-type crystalline pattern observed in XRD.

Table 6
Secondary structure composition of Glutelin protein under different treatments.

Parameters	Samples					
	F_1	F_2	F_3	F_4	F_5	F_6
α-Helix (%)	11.50 ± 0.25	11.50 ± 0.32	11.50 ± 0.40	11.50 ± 0.20	11.50 ± 0.45	11.50 ± 0.15
β-Sheet (%)	31.20 ± 0.35	31.20 ± 0.25	31.10 ± 0.25	31.20 ± 0.40	31.20 ± 0.10	31.20 ± 0.30
Turn (%)	14.90 ± 0.15	14.90 ± 0.20	14.90 ± 0.30	14.90 ± 0.25	14.90 ± 0.35	14.90 ± 0.10
Other Structures (%)	42.40 ± 0.05	42.40 ± 0.27	42.40 ± 0.45	42.40 ± 0.05	42.40 ± 0.50	42.40 ± 0.05

* Samples are reported as atmospheric cold plasma treated at 30s (F_1), 60s (F_2), 90s (F_3), 120s (F_4), parboiled samples (F_5) and control sample (F_6).

Conclusion

The results of this study demonstrated that atmospheric cold plasma (ACP) treatment significantly influences the surface properties and cooking behavior of *local Tarom* rice grains, with these effects being strongly dependent on the treatment duration. Notably, extending the treatment time up to 90 s, particularly in sample F3, resulted in a substantial improvement in cooking performance. In contrast, longer treatment durations, which can be considered harsh conditions, did not necessarily produce additional benefits, indicating that ACP treatment has an optimum exposure time. The improved behavior of F3 was mainly associated with surface modification, increased nanoscale roughness, and improved water accessibility, while XRD and CD analyses confirmed that the main starch crystalline pattern and glutelin secondary structure were largely preserved. Therefore, ACP can be considered a promising non-thermal strategy for improving selected technological properties of *Local Tarom* rice without the more severe color and hydrothermal changes associated with parboiling. Further studies should evaluate RVA parameters and sensory properties, because these analyses were not included in the present data set and are needed to confirm consumer-level quality and pasting behavior.

Data availability

All data supporting the findings of this study are included in this article and the accompanying tables and figures. Additional raw data are available from the corresponding authors on reasonable request.

Code availability

No custom computer code was used in this study.

Declarations

Competing Interests

This research received financial support from Shahid Sadoughi University of Medical Sciences, Yazd, Iran, as part of the corresponding thesis project. No grant number was assigned to this funding.

Funding

This research received financial support from Shahid Sadoughi University of Medical Sciences, Yazd, Iran, as part of the corresponding thesis project. No grant number was assigned to this funding.

Author Contribution

J.K. performed the investigation and drafted the manuscript. M.Z. and R.S. performed the literature search and data analysis. N.M.-M. and R.E.K. conceptualized the study. All authors reviewed and approved the final manuscript.All authors reviewed and approved the final version of the manuscript.

Acknowledgement

The authors would like to thank the School of Public Health, Shahid Sadoughi University of Medical Sciences, Yazd, Iran, for the financial support of this work. The authors are also grateful to the Industrial Agricultural Saffron Saharkhiz Group (Mashhad, Iran) for their valuable collaboration and support throughout the course of this research. This study was approved under the ethics code IR.SSU.SPH.REC.1404.033.

Data Availability

Data AvailabilityThe datasets generated during and/or analysed during the current study are available from the corresponding author on reasonable request.

References

1. Chen, H. H., Hung, C. L., Lin, S. Y. & Liou, G. J. Effect of low-pressure plasma exposure on the storage characteristics of brown rice. *Food Bioprocess Technol.* **8**, 471–477 (2015).
2. Misnal, M. F. I. et al. Emerging cold plasma treatment on rice grains: A mini review. *Chemosphere* **274**, 129972 (2021).
3. Adedeji, K., Raji, N., Oyetunji, E. & Ishola, B. Design and fabrication of a motorized rice hulling machine. *J. Mech. Eng. Res.* **11**, 1–10 (2020).
4. Akhter, K. T. et al. Variations in the major nutrient composition of dominant high-yield varieties (hyvs) in parboiled and polished rice of Bangladesh. *Foods* **12**, 3997 (2023).

5. Omar, S. C., Shaharudin, A. & Tumin, S. A. The status of the paddy and rice industry in Malaysia. *Khazanah Res. Inst. Kuala Lumpur* (2019).
6. Yodpitak, S. et al. Cold plasma treatment to improve germination and enhance the bioactive phytochemical content of germinated brown rice. *Food Chem.* **289**, 328–339 (2019).
7. Zhou, C. et al. Air and argon cold plasma effects on lipolytic enzymes inactivation, physicochemical properties and volatile profiles of lightly-milled rice. *Food Chem.* **445**, 138699 (2024).
8. Chen, Z. et al. Sorption equilibrium moisture and isosteric heat of cold plasma treated milled rice. *Innovative Food Sci. Emerg. Technol.* **55**, 35–47. https://doi.org/10.1016/j.ifset.2019.05.012 (2019).
9. Qiang, L. et al. Dielectric Barrier Discharge Cold Plasma Improves Storage Stability in Paddy Rice by Activating the Phenylpropanoid Biosynthesis Pathway. *J. Agric. Food Chem.* **72** 10.1021/acs.jafc.4c04316 (2024).
10. Akasapu, K., Ojah, N., Gupta, A. K., Choudhury, A. J. & Mishra, P. An innovative approach for iron fortification of rice using cold plasma. *Food Res. Int.* **136**, 109599. https://doi.org/10.1016/j.foodres.2020.109599 (2020).
11. Sarangapani, C., Devi, Y., Thirundas, R., Annapure, U. S. & Deshmukh, R. R. Effect of low-pressure plasma on physico-chemical properties of parboiled rice. *LWT-food Sci. Technol.* **63**, 452–460 (2015).
12. Karimi, J. et al. Harnessing Cold Plasma for Rice Grain Processing: A Systematic Review on Functional, Structural, and Nutritional Properties. *Compr. Rev. Food Sci. Food Saf.* **25**, e70409 (2026).
13. Gupta, R. K., Guha, P. & Srivastav, P. P. Effect of cold plasma treatment and plasma-activated water on physicochemical and structural properties of starch: A green and novel approach for environmental sustainability. *Plasma Processes Polym.* **21**, 2300204 (2024).
14. Ji, H., Li, D., Zhang, L., Li, M. & Ma, H. Effect of atmospheric pressure plasma jet on the structure and physicochemical properties of wheat starch. *Front. Nutr.* **11**, 1386778 (2024).
15. Hosseinpour, A., Fazaeli, M., Hedayati, S. & Niakousari, M. The impact of atmospheric nitrogen cold plasma on the granular cold-water swelling tapioca starch: structure and functionality. *Int. J. Food Prop.* **28**, 2569679 (2025).
16. Wani, A. A. et al. Rice Starch Diversity: Effects on Structural, Morphological, Thermal, and Physicochemical Properties—A Review. *Compr. Rev. Food Sci. Food Saf.* **11**, 417–436. 10.1111/j.1541-4337.2012.00193.x (2012).
17. Lin, X., Zhang, X., Du, B. & Xu, B. Morphological, structural, thermal, pasting, and digestive properties of starches isolated from different varieties of rice: A systematic comparative study. *Foods* **12**, 4492 (2023).
18. Mir, S. A. et al. Parboiling and milling properties. *Int. J. Food Eng.* **11**, 777–787 (2015).
19. Ojediran, J. O. et al. Effect of polishing duration on physical, milling, cooking, and sensory properties of a novel mix-colored Nigerian parboiled rice. *Cereal Chem.* **97**, 1172–1182 (2020).

20. Mudgal, S. & Singh, N. Effect of parboiling treatment times on the physicochemical, cooking, textural, and pasting properties and amino acid, phenolic, and sugar profiles of germinated paddy rice from different rice varieties. *J. Food Sci.* **89**, 3208–3229 (2024).
21. M, M., O, O. & A, A. & Effect of Degree of Milling on Proximate and Mineral Composition, Physicochemical, Colour Characteristics and Pasting Properties of Broken Brown Rice Fraction from a Selected Variety (FARO 64). *Afr. J. Agric. Food Sci.* 10.52589/ajafs-trp3xczj (2024).
22. Sivakamasundari, S., Moses, J. & Anandharamakrishnan, C. Effect of parboiling methods on the physicochemical characteristics and glycemic index of rice varieties. *J. Food Meas. Charact.* **14**, 3122–3137 (2020).
23. Tong, C., Gao, H., Luo, S., Liu, L. & Bao, J. Impact of Postharvest Operations on Rice Grain Quality: A Review. *Compr. Rev. Food Sci. Food Saf.* **18**, 626–640. 10.1111/1541-4337.12439 (2019).
24. Yussof, N. Y. S. M., Hong, S. P., Phuah, E. T. & Hassan, U. H. in *IOP Conference Series: Earth and Environmental Science.* 012003 (IOP Publishing).
25. Bandara, A., Batugahage, B., Prasantha, B. & Senanayake, D. Impact of amylose content on physical properties, cooking qualities, and water absorption of long-grain basmati-type rice (Oryza sativa L.) varieties. *Ceylon J. Science* **54** (2025).
26. Yao, F. et al. Effects of different cooking methods on glycemic index, physicochemical indexes, and digestive characteristics of two kinds of rice. *Processes* **11**, 2167 (2023).
27. Muchlisyiyah, J. et al. Parboiled rice processing method, rice quality, health benefits, environment, and future perspectives: A review. *Agriculture* **13**, 1390 (2023).
28. Cao, Z., Li, X., Song, H., Jie, Y. & Liu, C. Effect of intermittent low-pressure radiofrequency helium cold plasma treatments on rice gelatinization, fatty acid, and hygroscopicity. *Foods* **13**, 1056 (2024).
29. Liu, J., Wang, R., Chen, Z. & Li, X. J. Effect of Cold Plasma Treatment on Cooking, Thermomechanical and Surface Structural Properties of Chinese Milled Rice. *Food Bioprocess Technol.* **14**, 866–886. 10.1007/s11947-021-02614-1 (2021).
30. Uyeh, D. D., Woo, I. K. J. J., Ha, Y. S. & S. M. & Drying characteristics and milling quality of parboiled Japonica rice under various drying conditions. *Eng. Agric. Environ. Food*. **10**, 292–297 (2017).
31. Rattanamechaiskul, C., Junka, N. & Prakotmak, P. Modeling and optimization of moisture diffusion of paddy and brown rice during thermal soaking. *J. Food Process Eng.* 10.1111/jfpe.14302 (2023).
32. Billiris, M. A., Siebenmorgen, T. J. & Mauromoustakos, A. Estimating the theoretical energy required to dry rice. *J. Food Eng.* **107**, 253–261 (2011).
33. Xu, M. et al. Effects of starch gelatinisation and water migration on the hardness of parboiled rice. *Int. J. Food Sci. Technol.* **59**, 8708–8717 (2024).
34. Vidal, V. et al. Cooking behavior of rice in relation to kernel physicochemical and structural properties. *J. Agric. Food Chem.* **55**, 336–346 (2007).
35. Thirumdas, R., Deshmukh, R. & Annapure, U. Effect of low temperature plasma processing on physicochemical properties and cooking quality of basmati rice. *Innovative Food Sci. Emerg.*

Technol. **31**, 83–90 (2015).

36. Thirumdas, R., Saragapani, C., Ajinkya, M., Deshmukh, R. & Annapure, U. Influence of low pressure cold plasma on cooking and textural properties of brown rice. *Innovative Food Sci. Emerg. Technol.* **37**, 53–60 (2016).
37. Noppakun, M. et al. Effects of plasma treatment on cooking and physical qualities of pigmented Thai rice. CMUJ. *Nat. Sci.* **20**, e2021004 (2021).
38. Pal, P. et al. Effect of nonthermal plasma on physico-chemical, amino acid composition, pasting and protein characteristics of short and long grain rice flour. *Food Res. Int.* **81**, 50–57 (2016).
39. Thirumdas, R., Deshmukh, R. & Annapure, U. Effect of low temperature plasma on the functional properties of basmati rice flour. *J. Food Sci. Technol.* **53**, 2742–2751 (2016).
40. Chaple, S. et al. Effect of atmospheric cold plasma on the functional properties of whole wheat (Triticum aestivum L.) grain and wheat flour. *Innovative Food Sci. Emerg. Technol.* **66**, 102529 (2020).
41. Pozo, C. et al. Study of the structural order of native starch granules using combined FTIR and XRD analysis. *J. Polym. Res.* **25**, 266 (2018).
42. Taghavi, A., Nedamani, A. R., Motevali, A. & Hashemi, S. J. Expanding the Application of Potato Starch in Diverse Food Products by Modifying Its Water Absorption, Swelling, and Solubility Through Pregelatinization–Cold Plasma Treatments. *Journal of Food Biochemistry* 6809100 (2025). (2025).
43. Fang, J., Fowler, P., Tomkinson, J. & Hill, C. The preparation and characterisation of a series of chemically modified potato starches. *Carbohydr. Polym.* **47**, 245–252 (2002).
44. Nzenguet, A. M. et al. Novel bionanocomposite films based on graphene oxide filled starch/polyacrylamide polymer blend: structural, mechanical and water barrier properties. *J. Polym. Res.* **25**, 86 (2018).
45. Thirumdas, R., Trimukhe, A., Deshmukh, R. & Annapure, U. Functional and rheological properties of cold plasma treated rice starch. *Carbohydr. Polym.* **157**, 1723–1731 (2017).
46. Govindaraju, I. et al. Investigation of structural and physico-chemical properties of rice starch with varied amylose content: A combined microscopy, spectroscopy, and thermal study. *Food Hydrocoll.* **122**, 107093 (2022).
47. Gupta, R. K., Guha, P. & Srivastav, P. P. Effect of high voltage dielectric barrier discharge (DBD) atmospheric cold plasma treatment on physicochemical and functional properties of taro (Colocasia esculenta) starch. *Int. J. Biol. Macromol.* **253**, 126772 (2023).
48. Zhu, Q. et al. Hierarchical structural modification of starch via non-thermal plasma: A state-of-the-art review. *Carbohydr. Polym.* **311**, 120747 (2023).
49. Tian, J. et al. Parboiling reduced the crystallinity and in vitro digestibility of non-waxy short grain rice. *Food Chem.* **257**, 23–28 (2018).
50. Derycke, V. et al. Starch gelatinization and amylose–lipid interactions during rice parboiling investigated by temperature resolved wide angle X-ray scattering and differential scanning calorimetry. *J. Cereal Sci.* **42**, 334–343 (2005).

51. Sittipod, S. & Shi, Y. C. Changes of starch during parboiling of rice kernels. *J. Cereal Sci.* **69**, 238–244 (2016).
52. Sanjana Potluri, S. P., Sangeetha, K., Santhosh, K. S. R. & Nivas, R. S. G. G. N. & Radhakrishnan Mahendran, R. M. Effect of low-pressure plasma on bamboo rice and its flour. (2018).
53. Shin, Y. & Yoo, D. I. Surface characterization of PET nonwoven fabric treated by He/O2 atmospheric pressure plasma. *J. Appl. Polym. Sci.* **108**, 785–790 (2008).
54. Klébert, S. et al. Degradation phenomena on atmospheric air plasma treatment of polyester fabrics. *Surf. Interfaces*. **22**, 100826 (2021).
55. Oguzlu, H. et al. Cold plasma for the modification of the surface roughness of microparticles. *ACS omega*. **9**, 35634–35644 (2024).
56. Ayoub, A., Ohtani, T. & Sugiyama, S. Atomic force microscopy investigation of disorder process on rice starch granule surface. *Starch-Stärke* **58**, 475–479 (2006).
57. Jiao, Y. et al. Effect of the surface peak-valley features on droplet splash dynamics. *Physics Fluids* **35** (2023).
58. Rey-Stolle, I., Barrigon, E., Galiana, B. & Algora, C. Analysis of germanium epiready wafers for III–V heteroepitaxy. *J. Cryst. Growth.* **310**, 4803–4807 (2008).
59. Mateescu, A. O. et al. Stainless steel surface nitriding in open atmosphere cold plasma: Improved mechanical, corrosion and wear resistance properties. *Materials* **14**, 4836 (2021).
60. Czerwiec, T., Tsareva, S., Andrieux, A., Bruyere, S. & Marcos, G. Effects of surface topography at different scales on the dispersion of the wetting data for sessile water droplets on nitrided austenitic stainless steels. *Surf. Coat. Technol.* **441**, 128510 (2022).
61. Wongsue, S. et al. Effect of surface topography and wettability on shear bond strength of Y-TZP ceramic. *Sci. Rep.* **13**, 18249 (2023).
62. Lamberts, L., Brijs, K., Mohamed, R., Verhelst, N. & Delcour, J. A. Impact of browning reactions and bran pigments on color of parboiled rice. *J. Agric. Food Chem.* **54**, 9924–9929 (2006).
63. Lamberts, L. et al. Effect of processing conditions on color change of brown and milled parboiled rice. *Cereal Chem.* **83**, 80–85 (2006).
64. Bhattacharya, S. Kinetics on colour changes in rice due to parboiling. *J. Food Eng.* **29**, 99–106 (1996).
65. Lee, K. H. et al. Evaluation of cold plasma treatments for improved microbial and physicochemical qualities of brown rice. *Lwt* **73**, 442–447 (2016).
66. Chen, H. H., Chen, Y. K. & Chang, H. C. Evaluation of physicochemical properties of plasma treated brown rice. *Food Chem.* **135**, 74–79 (2012).
67. Okyere, A. Y., Rajendran, S. & Annor, G. A. Cold plasma technologies: Their effect on starch properties and industrial scale-up for starch modification. *Curr. Res. Food Sci.* **5**, 451–463 (2022).
68. Ge, X. et al. The improving effects of cold plasma on multi-scale structure, physicochemical and digestive properties of dry heated red adzuki bean starch. *Food Chem.* **349**, 129159 (2021).

69. Greenfield, N. J. Using circular dichroism spectra to estimate protein secondary structure. *Nat. Protoc.* **1**, 2876–2890 (2006).
70. Quddus, K. & Ching-Yung, M. Study of rice glutelins conformation by using circular dichroism (CD) spectroscopy. *Pakistan J. Biol. Sci. (Pakistan)* 6 (2003).
71. Held, S., Tyl, C. E. & Annor, G. A. Effect of radio frequency cold plasma treatment on intermediate wheatgrass (Thinopyrum intermedium) flour and dough properties in comparison to hard and soft wheat (Triticum aestivum L.). *Journal of Food Quality* 1085172 (2019). (2019).
72. Warne, G. R. et al. Impact of cold plasma on the biomolecules and organoleptic properties of foods: A review. *J. Food Sci.* **86**, 3762–3777 (2021).
73. Olatunde, O. O. et al. Cold atmospheric plasma-induced protein modification: Novel nonthermal processing technology to improve protein quality, functionality, and allergenicity reduction. *Compr. Rev. Food Sci. Food Saf.* **22**, 2197–2234 (2023).

Figures

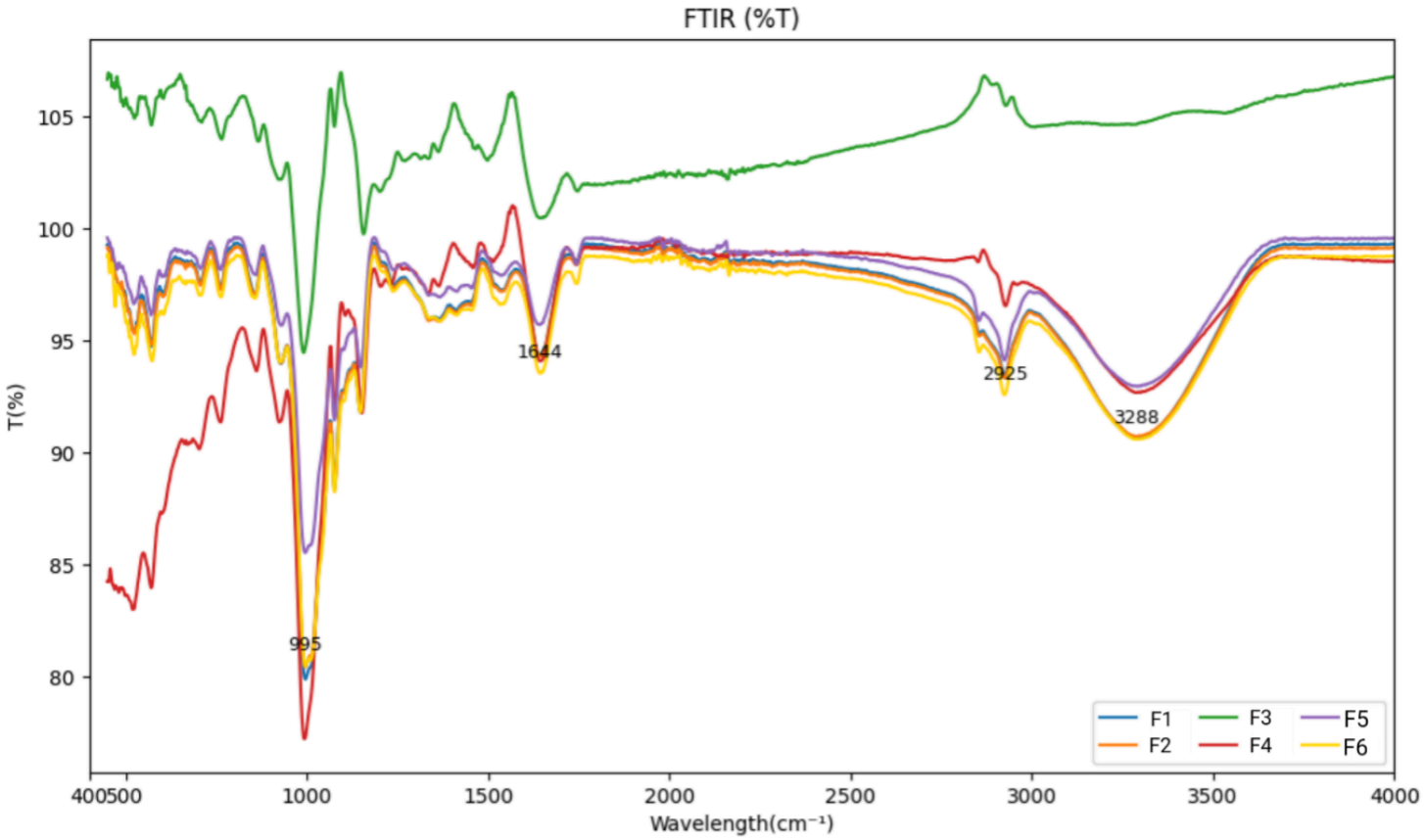


Figure 1

FTIR spectra of treated rice samples. F1–F4 denote samples treated with atmospheric cold plasma for 30, 60, 90, and 120 s, respectively; F5 denotes the parboiled sample; and F6 denotes the untreated control. FTIR, Fourier-transform infrared spectroscopy; %T, percent transmittance.

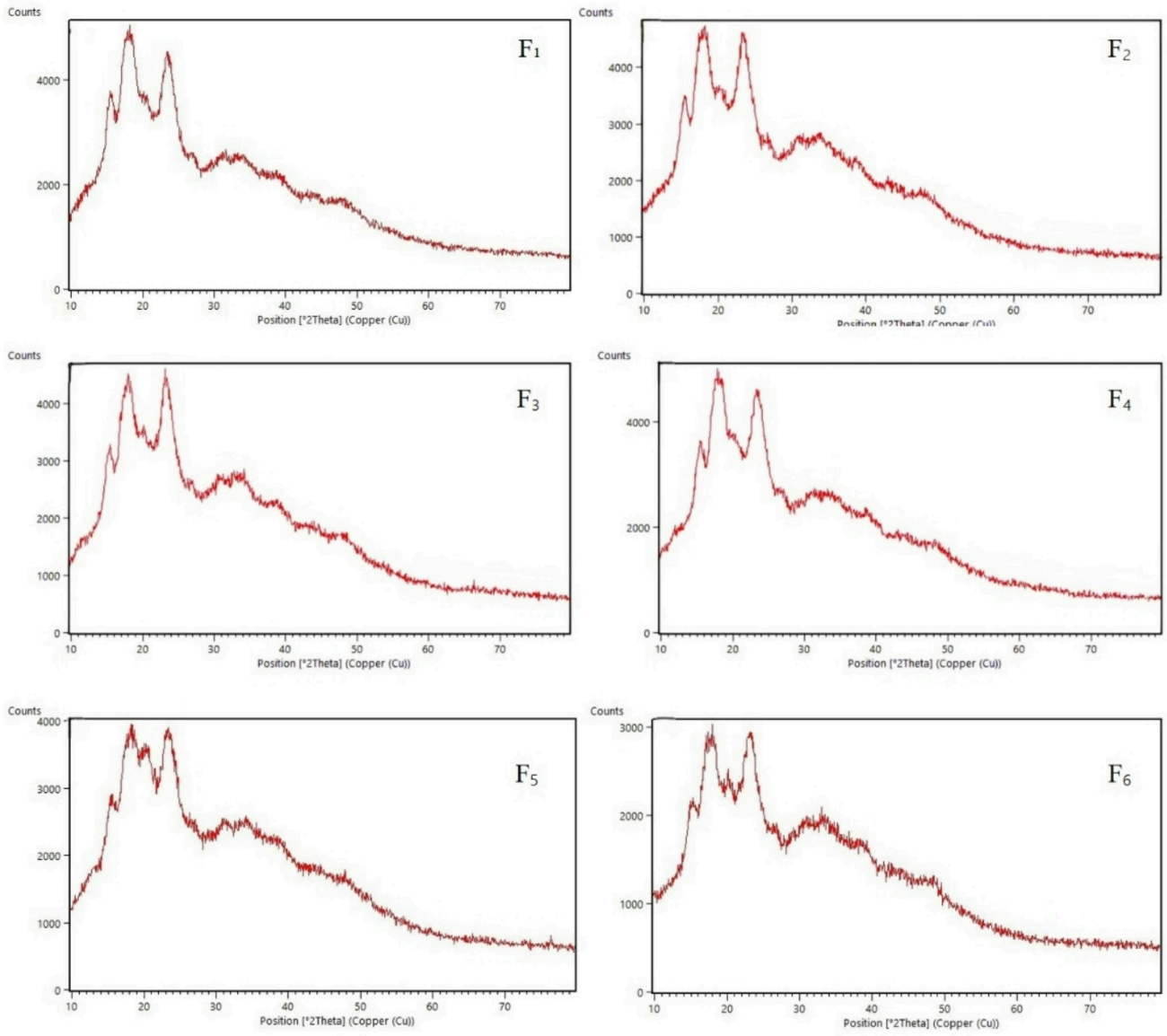


Figure 2

X-ray diffraction patterns of treated rice samples. F1–F4 denote samples treated with atmospheric cold plasma for 30, 60, 90, and 120 s, respectively; F5 denotes the parboiled sample; and F6 denotes the untreated control. XRD, X-ray diffraction.

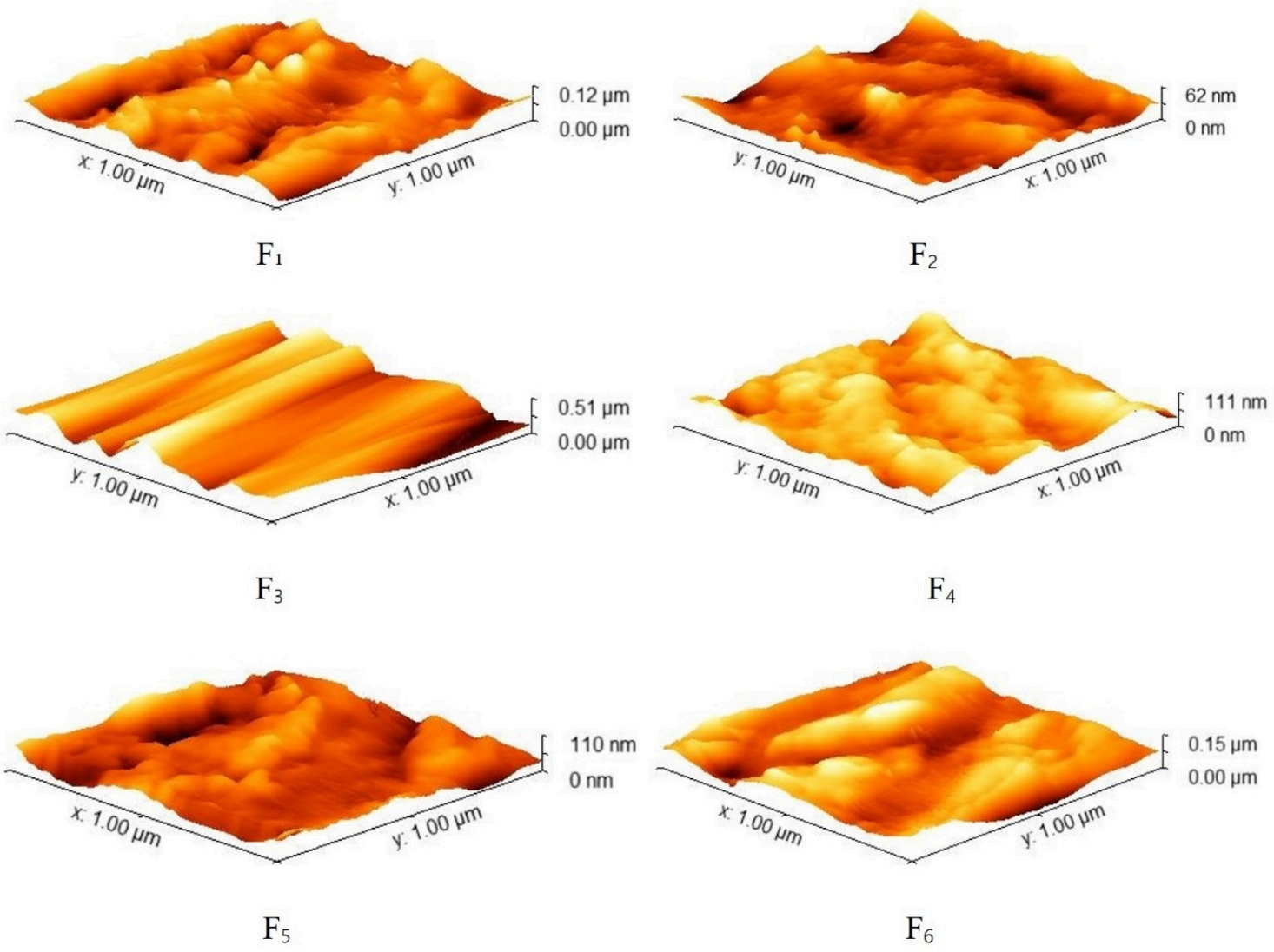


Figure 3

Atomic force microscopy topographs of treated rice samples. Representative images from three independent measurements are shown over a 1 × 1 µm scan area; labels beside each panel indicate the vertical height range. F1–F4 denote samples treated with atmospheric cold plasma for 30, 60, 90, and 120 s, respectively; F5 denotes the parboiled sample; and F6 denotes the untreated control.

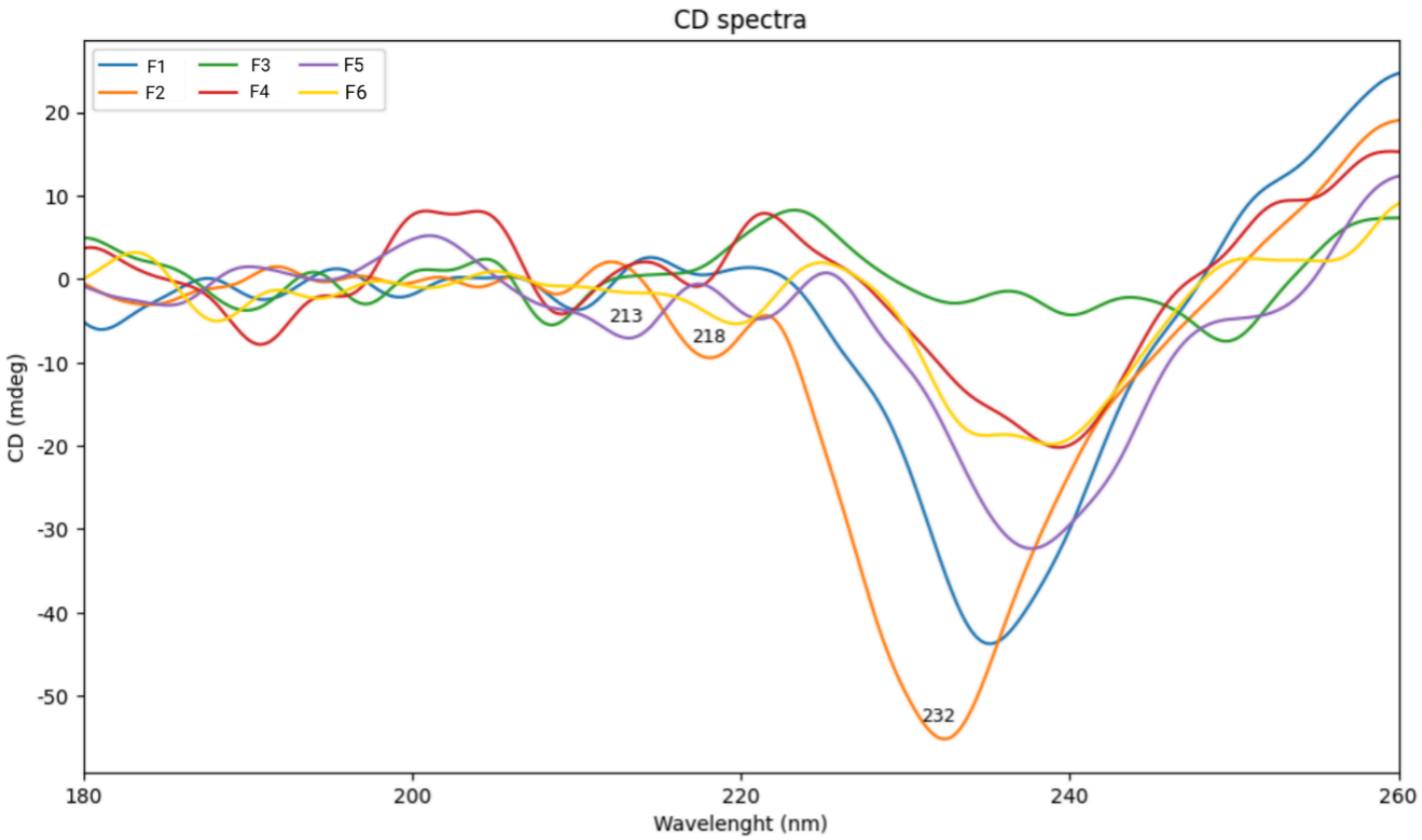


Figure 4

Far-UV circular dichroism spectra of glutelin extracted from treated rice samples. Spectra were recorded from 176 to 260 nm. F1–F4 denote samples treated with atmospheric cold plasma for 30, 60, 90, and 120 s, respectively; F5 denotes the parboiled sample; and F6 denotes the untreated control. CD, circular dichroism.

Supplementary Files

This is a list of supplementary files associated with this preprint. Click to download.

- CreditauthorStatement.docx
- DeclarationofCompetingInterest.docx
- graficalabstract.png
- Highlight.docx